Food Chemistry 506 (2026) 148198

Contents lists available at ScienceDirect

Food Chemistry

journal homepage: www.elsevier.com/locate/foodchem

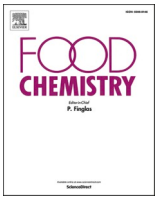

Functionalized carbon nanotube-based affinity chromatography for polyphenol oxidase purification from different sources and evaluation of kinetic properties

Mehmet Doğan [a,*,1], Fatma Nur Yalçinkaya [a,2], Zeynep Bicil [a,3], Berna Koçer Kizilduman [a,4], Serap Doğan [b,5]

[a] Balikesir University Faculty of Science and Literature Department of Chemistry, 10145 Balikesir, Turkey
[b] Balikesir University Faculty of Science and Literature Department of Molecular Biology and Genetics, 10145 Balikesir, Turkey

ARTICLE INFO

Keywords:
Polyphenol oxidase
Affinity chromatography
Multi-walled carbon nanotubes
Enzyme purification
Enzyme kinetics

ABSTRACT

In this study, functionalized multi-walled carbon nanotubes (MWCNT) were firstly synthesized and applied to purify polyphenol oxidase (PPO). Structural characterization of matrix was confirmed via different techniques. BET surface area decreased from 278.0 to 202.8 $m^2 \cdot g^{-1}$ with functionalization. Affinity chromatography achieved 16.4-fold purification for *S. officinalis* L., 12.9-fold purification for mushroom, 8.4-fold for *S. aethiopis* L., while SDS-PAGE analysis of *S. officinalis* L. revealed a single distinct band corresponding to an estimated molecular weight of approximately 43–45 kDa. **Optimum pH and temperature values varied depending on the substrates and purification step.** Kinetic analysis revealed substrate-dependent catalytic behavior, with catechol (K_M = 0.0035–0.0050 mM; V_{max} = 5.000–25.000 EU/mL), 4-methylcatechol (K_M = 0.00129–0.00333 mM; V_{max} = 10.000–14.286 EU/mL) and pyrogallol (K_M = 0.00075–0.0040 mM; V_{max} = 5.000–50.000 EU/mL). Pyrogallol showed the highest catalytic activity due to its high V_{max}/K_M value. **These results highlight the potential of functionalized MWCNTs as effective affinity supports for PPO purification and position Salvia species and mushroom as a promising natural enzyme source for industrial and biotechnological applications.**

1. Introduction

In today's world, where technological advancements increasingly shape critical areas such as biotechnology and food science, traditional purification techniques often fall short of delivering the selectivity, efficiency, and scalability required for modern applications. This challenge has driven the development of multifunctional and high-performance materials capable of enhancing enzyme purification processes (Çakır et al., 2021; Yalçınkaya et al., 2024; Hussein et al., 2019). Polyphenol oxidases (PPOs; EC 1.14.18.1) are copper-containing oxidoreductase enzymes widely found in plants, animals, and microorganisms. They catalyze the oxidation of o-diphenols to o-quinones, which subsequently polymerize into dark pigments, leading to enzymatic browning in fruits, vegetables, and other plant-based foods. Although this reaction plays a protective role in plant defense, it often causes undesirable color, flavor, and nutritional changes in food products, posing a major problem in food processing and storage (Doğan et al., 2007; Doğan et al., 2009; Doğan et al., 2013; Gomes et al., 2014).

Understanding the structure, catalytic behavior, and inhibition mechanisms of PPOs is crucial for developing effective strategies to control enzymatic browning and for exploring their potential use in biotechnological and industrial applications. However, purification of

* Corresponding author.
E-mail addresses: mdogan@balikesir.edu.tr (M. Doğan), zeynepbicil@balikesir.edu.tr (Z. Bicil), bernakocer@balikesir.edu.tr (B.K. Kizilduman), sdogan@balikesir.edu.tr (S. Doğan).
[1] 0000–0002–3707-0497
[2] **0000–0003–2981-8095**
[3] **0000–0002-5023-947**×
[4] **0000–0002–0826-3556**
[5] 0000–0001–5684-3662

https://doi.org/10.1016/j.foodchem.2026.148198
Received 26 July 2025; Received in revised form 25 December 2025; Accepted 26 January 2026
Available online 28 January 2026

PPOs is often challenging due to their membrane-bound nature, low abundance, and presence of multiple isoenzymes. Conventional purification methods, including ammonium sulfate precipitation, dialysis, gel filtration, and ion-exchange chromatography, can partially purify the enzyme but are typically time-consuming, labor-intensive, and may cause activity loss (Doğan et al., 2005; Şakiroğlu, 1994; Zou et al., 2024). Therefore, there is a strong need to develop more efficient, selective, and economical purification strategies. Affinity chromatography is recognized as one of the most effective purification techniques, offering high specificity and resolution. In recent years, the integration of nanomaterials into affinity systems has drawn considerable attention due to their unique physicochemical properties, which allow for improved selectivity and binding efficiency.

Carbon nanotubes (CNTs) are one-dimensional nanostructures composed of graphene layers rolled into cylindrical shapes, known for their high surface area, remarkable mechanical strength, and tunable surface chemistry (Bicil, 2026). These features enable strong interactions with biomolecules through π–π stacking, hydrogen bonding, and electrostatic attractions. However, pristine CNTs lack reactive surface groups, which limits their chemical reactivity and interaction with biomolecules. This limitation was clearly demonstrated in the study by Mohammadi et al. (2009), where the adsorption behavior and electrochemical properties of PPO on unmodified SWCNTs were investigated, but low adsorption efficiency was observed due to the absence of functional groups on the nanotube surfaces. These findings underscore the necessity of surface modification to improve binding interactions and enzyme immobilization performance (Mohammadi et al., 2009). To overcome this limitation, functionalization of CNTs with chemical groups such as –COOH, –OH, and –NH_2 enhances biocompatibility and selective adsorption capacity, making them promising materials for enzyme purification and immobilization (Gomes et al., 2014; Ombaka et al., 2014; Oyetade et al., 2015). Multi-walled carbon nanotubes (MWCNTs), with their multiple concentric graphene layers, provide structural robustness, high binding site density, and easy regeneration, making them suitable as affinity matrix supports (Çam et al., 2025). Compared to traditional matrices like Sephadex/Sepharose-based gels, MWCNT-based supports can offer higher adsorption capacity, reusability, and cost-effectiveness. Furthermore, functionalized MWCNTs are well-established in electrochemical biosensing, where high surface area and graphitic π-systems, combined with tailored surface chemistries, enable stable and oriented enzyme immobilization with reduced nonspecific adsorption under mild conditions. Translating these interface principles to purification provides three levers: higher capture probability on π-active, high-site-density surfaces; ligand–spacer–guided selectivity; and gentle, activity-preserving elution (Dubey et al., 2021; Oskin et al., 2023; Wee et al., 2019).

The Lamiaceae family comprises a wide range of aromatic and medicinal plants rich in phenolic compounds, flavonoids, and essential oils, which contribute to antioxidant and enzymatic activities. Among its genera, Salvia is particularly notable for its high PPO activity**. A wild species, *Salvia aethiopis* L., and *Salvia officinalis* L., are characterized by abundant phenolic compounds and strong enzymatic potential, making it an attractive source for PPO extraction and studies** (Dorman et al., 2004; Kürkcüoğlu et al., 2001; Çatak & Atalay, 2022)**.** Mushrooms are widely used as classical model systems for studying PPO-mediated enzymatic browning, as polyphenol oxidase plays a central role in the oxidation of phenolic substrates and subsequent quality deterioration (Ma et al., 2025). Despite numerous reports on PPOs from various sources (Çam et al., 2025; Doğan et al., 2005, Doğan et al., 2009, Doğan et al., 2013), to the best of our knowledge, no study has yet combined nanostructured carbon materials with affinity chromatography for PPO purification from *Salvia aethiopis* L., ***Salvia officinalis*** L. **and mushroom.** In this regard, functionalized MWCNTs represent a novel generation of affinity matrices, uniting highly reactive nanostructured surfaces with specific enzyme-binding capacity. In the present study, a chemically functionalized MWCNT-based affinity matrix was designed and employed for the purification of PPO from the leaves and flowers of *Salvia aethiopis* L., the leaves of ***Salvia officinalis*** L. and mushroom. The purification performance was evaluated in terms of specific activity, purification fold, and yield, while kinetic parameters were determined using catechol, 4-methylcatechol, and pyrogallol as substrates. PPO from *S. aethiopis* L. was successfully purified and its kinetic properties characterized, while the synthesized affinity matrix was further evaluated using *S. officinalis* L. PPO to assess its selectivity. This nanomaterial-based strategy offers a reusable, cost-effective, and efficient alternative to conventional purification techniques, contributing to the advancement of nanomaterial-assisted enzyme purification technologies.

2. Materials and methods

2.1. Materials

MWCNT used in the study was purchased from Nanografi company (99% purity); polyethylene glycol from Sigma-Aldrich. Other all chemical reagents were of analytical grade, commercially obtained, and used without any further purification. The plant sample useds as the biological source for the purification of PPO belong to the Lamiaceae family and *Salvia aethiopis* L. was collected in May 2023 and ***Salvia officinalis*** L. in November 2025 from the Balıkesir province of Turkey. The mushroom was purchased from a local market in Balıkesir. The Salvia plants were taxonomically authenticated by Prof. Dr. Serap Doğan and stored at −70 °C at the BAUN Chemistry Laboratory to ensure traceability.

2.2. Hydroxylation of MWCNTs

For the synthesis of hydroxyl-functionalized multi-walled carbon nanotubes (MWCNT-OH), 0.5 g of MWCNTs was mixed with 30 mL of 0.3 M $FeCl_2 \bullet 4H_2O$ solution in a round-bottom flask. The mixture was subjected to ultrasonic treatment (Elmasonic S 40H, 220–240 V, 37 kHz, 340 W) in a water bath at 30 °C for 1 h. Subsequently, the mixture was transferred to a magnetic stirrer (Heidolph Magnetic Hotplate Stirrer, 250 rpm), and 30% H_2O_2 solution was added dropwise to a final volume of 120 mL. After the addition was completed, the system was stirred continuously at room temperature for 12 h using a magnetic stirrer. Following the reaction, the resulting suspension was filtered, and the solid phase was washed several times with 5% HCl solution, followed by deionized water until the pH became neutral (pH ≈ 7). The washed solid product was dried in an oven at 60 °C for 24 h and labeled as "MWCNT-OH" (Gao et al., 2017; Yanmaz et al., 2021). The reaction scheme for this process is shown in Fig. 1a.

2.3. Synthesis of MWCNT-O-L-tyrosine-p-Aminobenzoic acid

The functionalized MWCNT-OH was activated using cyanogen bromide (CNBr) to render it reactive. The activated product was washed with 250 mL of ice-cold 0.1 M $NaHCO_3$ buffer and transferred to a beaker. Separately, a solution containing 80 mg of L-tyrosine dissolved in 20 mL of 0.1 M $NaHCO_3$ buffer was prepared and added to the beaker containing the activated MWCNT-OH suspension. This mixture was stirred continuously at 4 °C for 16 h to allow the reaction to proceed. After the reaction, unbound tyrosine in the solution was removed by thorough washing with distilled water. The filtrate containing tyrosine-bound nanotubes was then added to 40 mL of 0.2 M $NaHCO_3$ buffer. At this stage, 25 mg of p-aminobenzoic acid was dissolved in 10 mL of 1 M HCl in an ice bath. In a separate solution, 75 mg of $NaNO_2$ was dissolved in 5 mL of water and added dropwise to the inhibitor solution at 0 °C to initiate the diazotization reaction. The reaction mixture was allowed to stand for 10 min.

The diazotized inhibitor solution was then added to the previously prepared 40 mL MWCNT-L-tyrosine suspension. During the reaction, the

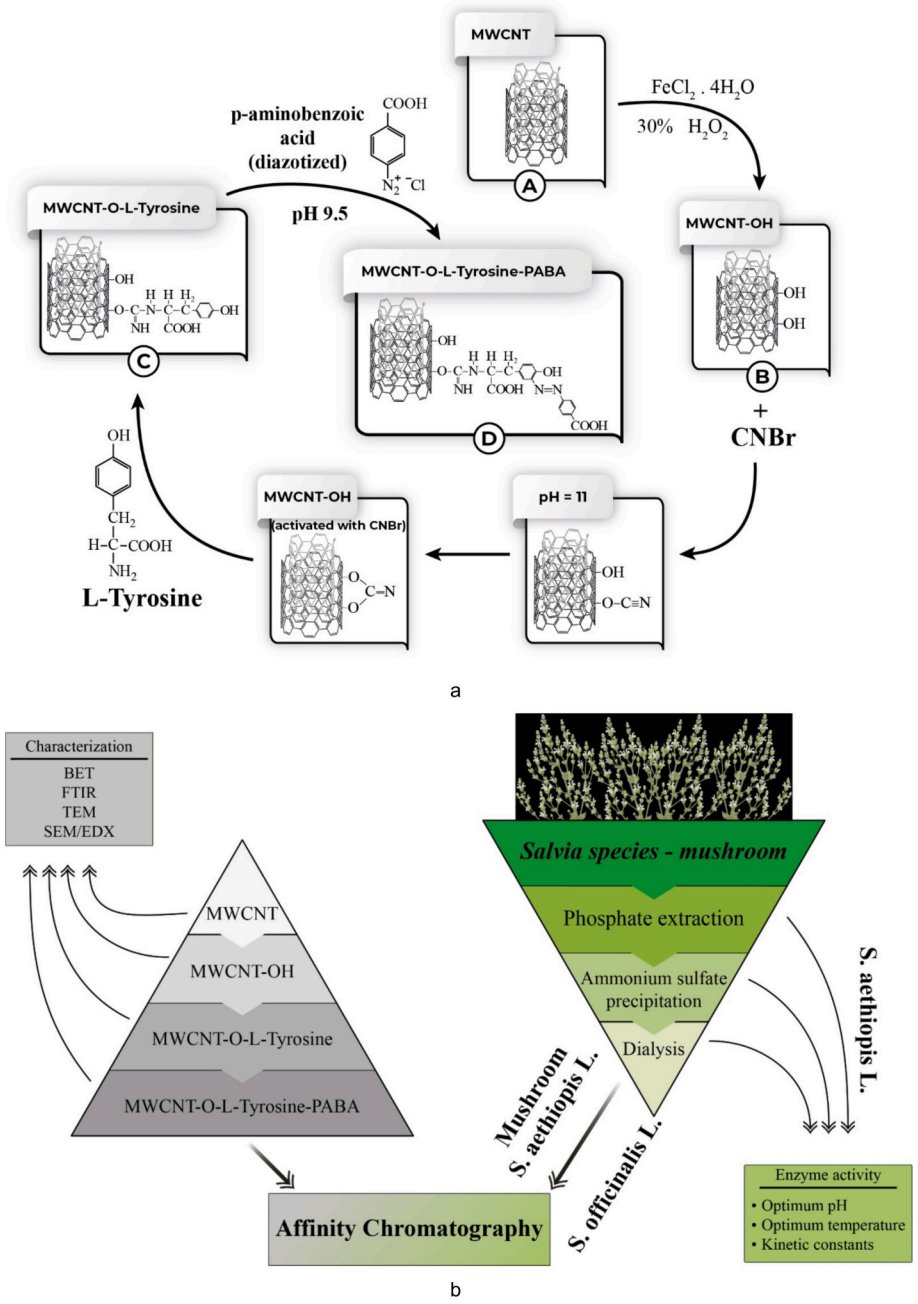

Fig. 1. a) the synthesis of MWCNT-O-L-tyrosine-p-aminobenzoic acid from MWCNTs and b) the flow diagram summarizing all experimental steps of the study

pH of the medium was maintained at 9.5 using 1 M NaOH, and the mixture was gently stirred at room temperature for 3 h. Upon completion, the product was washed with 1 L of distilled water followed by 200 mL of 0.05 M Tris-SO_4 buffer (pH 7.4) to achieve purification. The final product was collected and stored in the same buffer solution. The reaction scheme for this synthesis is presented in Fig. 1a (Doğan et al., 2005; Whitney, 1974).

2.4. Characterization

Characterization studies were conducted to determine the structural, surface, and morphological properties of the modified MWCNTs obtained after the functionalization process. For this purpose, FTIR, BET, SEM/EDX, and TEM analytical techniques were employed.

2.4.1. FTIR analysis

Fourier Transform Infrared Spectroscopy (FTIR) was performed using a PerkinElmer Spectrum 100 spectrometer to identify surface functional groups on the samples. Spectra were recorded in the 650–4000 cm^{-1} range.

2.4.2. BET surface area and pore size distribution

BET analysis was performed to determine the specific surface area and pore structure of the samples. Prior to analysis, all samples were degassed under vacuum at 100 °C for 24 h. Subsequently, surface areas and pore volumes were measured using nitrogen gas as the adsorbate in a liquid nitrogen environment (77 K). The measurements were carried out using a Quantachrome Nova 2200e surface area analyzer.

2.4.3. SEM/EDX analysis

Scanning Electron Microscopy (SEM) and Energy Dispersive X-ray

Spectroscopy (EDX) were utilized to examine the morphological structure and surface elemental distributions of the samples. SEM images were obtained using a Zeiss EVO LS10 microscope, while Bruker EDX analysis was used to determine the elemental composition of the sample surfaces at 20 kV.

2.4.4. TEM analysis

TEM images were obtained using a JEOL JEM-1400 Plus transmission electron microscope operating at an accelerating voltage of 120 kV. For sample preparation, 10 mg of the carbon-based material was dispersed in 10 mL of toluene. From this suspension, 10 μL was added to 10 mL of ethanol. Then, 10 μL of the resulting mixture was dropped onto a carbon-coated TEM grid. The solvent was evaporated by placing the grid in an oven at 60 °C for 1 h, after which the samples were ready for imaging.

2.5. Purification of PPO

2.5.1. Preparation of crude extract

Prior to extraction, PPO sources were treated with liquid nitrogen to facilitate the breakdown of cell wall-associated cellulose structures. Aliquots of 10 g of the liquid nitrogen-treated plant material were homogenized in 100 mL of 0.1 M phosphate buffer (pH 6.5) containing 5% polyethylene glycol and 10 mM ascorbic acid. The extraction was performed using a Waring blender for 2 min. The resulting homogenate was first filtered, and the filtrate was then centrifuged at 20,000 ×*g* (Sigma 3 K30) for 30 min at 4 °C to obtain the crude extract containing PPO (Doğan et al., 2005).

2.5.2. Ammonium sulfate precipitation

Preliminary screening of ammonium sulfate at 4 °C indicated that 80% saturation maximized post-dialysis activity recovery and specific activity. This choice is in good agreement with previous PPO/tyrosinase reports using 80% saturation (Doğan et al., 2005). To fractionate the soluble proteins in the crude extract, ammonium sulfate precipitation was performed up to 80% saturation. The required amount of ammonium sulfate was calculated using the following equation:

$$g\ (NH_4)_2SO_4 = \frac{1.77 \bullet V \bullet (S_2 - S_1)}{3.54 - S_2} \quad (1)$$

where V is the volume of the supernatant (mL), S_1 is the initial ammonium sulfate saturation (in decimal form), and S_2 is the target saturation level (Arslan et al., 2004). The calculated amount of ammonium sulfate was gradually added to the extract to reach 80% saturation. The resulting suspension was centrifuged at 20,000 ×*g* for 30 min at 4 °C, and the precipitate was collected while the supernatant was discarded.

2.5.3. Dialysis

The precipitate obtained after ammonium sulfate precipitation was redissolved in a small volume of 0.1 M phosphate buffer (pH 6.5). The solution was dialyzed for two days against 0.05 M phosphate buffer (pH 7.0), with the buffer replaced three times during the process using membrane dialysis (Doğan & Doğan, 2004).

2.5.4. Affinity chromatography

To achieve further purification of the PPO enzyme, affinity chromatography was performed. For this purpose, the synthesized modified MWCNT-based matrix was used as the column packing material. In this matrix, L-tyrosine served as the spacer arm of the affinity gel, while p-aminobenzoic acid (PABA) acted as the inhibitor unit responsible for specific enzyme binding (Arslan et al., 2004). The affinity matrix was packed into a Sigma double-jacketed column (bed volume 4 mL, I.D. × L 0.7 cm × 10 cm) to maintain thermal stability.

Column equilibration was carried out using 0.05 M acetate buffer (pH 5.0), which provides effective buffering capacity in this acidic pH range. The buffer was loaded from the top of the column and collected from the bottom until the absorbance at 280 nm dropped to 0.002, ensuring the removal of unbound components. After equilibration, the dialyzed enzyme solution was loaded onto the column. Washing with the same buffer continued to allow the binding of PPO to the affinity matrix while removing non-specifically bound impurities.

The binding of PPO to the functionalized MWCNT-based affinity matrix relies on reversible affinity forces, including electrostatic interactions, hydrogen bonding, π–π stacking, and inhibitor-mimetic recognition. While these interactions are maximized under acidic pH (5.0) conditions, shifting the pH to 7.0 alters the enzyme surface charge and binding energy, thereby allowing PPO to be eluted under mild conditions.

Elution was performed using 0.05 M phosphate buffer adjusted to pH 7.0, where the phosphate buffer system exhibits optimal buffering capacity, and eluates were collected in 2 mL Eppendorf tubes. Protein quantification and enzyme activity assays were conducted for each fraction. Using the obtained data, the specific activity, yield, and purification ratio of the PPO solution were calculated according to the following formulas:

$$\text{Specific activity} = \frac{\text{Total activity of the concentrated enzyme (EU)}}{\text{Total protein (mg)}} \quad (2)$$

$$\text{Yield (\%)} = \frac{\text{Total activity of the concentrated enzyme (EU)}}{\text{Total activity of the crude enzyme (EU)}} \times 100 \quad (3)$$

$$\text{Purification ratio} = \frac{\text{Specific activity of the concentrated enzyme (EU/mg)}}{\text{Specific activity of the crude enzyme (EU/mg)}} \quad (4)$$

With these calculations, purification efficiency, enzyme stability and purity level at each step were evaluated quantitatively.

2.5.5. Electrophoresis

SDS-PAGE analysis was performed using a standard discontinuous gel electrophoresis system (Bio-Rad Mini-PROTEAN). Protein samples were mixed with a denaturing sample buffer composed of Tris-HCl (0.5 M, pH 6.8), glycerol (10%, *v*/v), SDS (2%, *w/v*), β-mercaptoethanol (5%, v/v) and Coomessie stain (0.01%, w/v). The mixtures were then heated at 95 °C for 10 min to ensure complete denaturation. Subsequently, the samples were loaded onto 10% polyacrylamide resolving gels and separated under constant voltage. After electrophoresis, proteins were visualized using a silver staining procedure. Molecular mass estimations were carried out by comparison with a commercially available SDS-PAGE protein standard (Sigma) (Chazarra et al., 2001).

2.6. Kinetic characterization of PPO

2.6.1. pH optimization

The pH dependence of the enzymatic reaction was evaluated using different buffer systems covering the pH range of 4.0 to 9.0. Acetate buffer was used in the pH range of 4.0–6.0, and phosphate buffer was used in the pH range of 6.5–9.0. The pH of the buffer solutions was adjusted using 0.1 M NaOH and 0.1 M HNO_3 or HCl solutions. PPO enzyme activity was determined by measuring the increase in absorbance associated with product formation. The measurements were performed using a PerkinElmer Lambda 25 UV–Visible spectrophotometer. For enzyme activity assays, the increase in absorbance over a reaction period of 2 min was monitored at 420 nm for catechol and 4-methylcatechol substrates, and at 320 nm for the pyrogallol substrate. All spectrophotometric measurements were carried out in quartz cuvettes with a 1 cm light path, and the total reaction volume was kept constant at 3 mL for each experiment. One enzyme unit (EU) was defined as the amount of enzyme that causes an absorbance change of 0.001 per

minute under the assay conditions. The pH value at which the highest activity was observed for each substrate was considered the optimum pH (Doğan et al., 2002).

2.6.2. Temperature optimization

Enzyme activity was determined at the optimum pH over a temperature range of 20–50 °C. The measurements were performed using a UV–Visible spectrophotometer integrated with a temperature-controlled Peltier system. During the preparation of the reaction mixture, the enzyme solution was added once the quartz cuvette had reached the target temperature. In assays conducted with catechol, 4-methylcatechol, and pyrogallol as substrates, the total reaction volume was maintained at 3 mL (Doğan et al., 2005). The optimum temperature was determined by comparing the activity values obtained at each temperature.

2.6.3. Enzyme kinetics

Catechol, 4-methylcatechol, and pyrogallol at various concentrations were used as substrates in the kinetic analyses. The kinetic experiments were conducted under the enzyme's optimum pH and temperature conditions. The Michaelis-Menten constant (K_M) and maximum reaction rate (V_{max}) were calculated using the Lineweaver–Burk plot (Doğan et al., 2006 and 2008).

2.7. Protein determination

The total protein content was determined using the Bradford colorimetric method. Bovine Serum Albumin was used as the standard protein (Bradford, 1976). The protein concentrations obtained by this method were used in the calculations of specific activity and purification fold. A flow diagram summarizing all experimental steps of the study is presented in Fig. 1b.

3. Results and discussion

3.1. Characterization of MWCNTs and functionalized MWCNTs

3.1.1. FTIR analysis

The FTIR spectra presented in Fig. 2 contain characteristic bands that confirm the successful progression of each sequential functionalization step of the MWCNTs. In the spectrum of pristine MWCNTs (A), the band observed at 1554 cm^{-1} corresponds to C═C stretching vibrations, indicating the preservation of the nanotube's graphitic structure (Vesali Naseh et al., 2009). In the spectrum of hydroxylated MWCNTs (MWCNT-OH), (B), the band at 3439 cm^{-1} confirms the presence of –OH groups, while the bands at 2922 and 2844 cm^{-1} are attributed to aliphatic C—H stretching vibrations. Additionally, the band at 1168 cm^{-1} is associated with –OH bending vibrations of adsorbed water, and the band at 1559 cm^{-1} further confirms the retention of the nanotube's C═C skeletal structure (Tiwari & Singh, 2007). In the spectrum of the sample modified with L-tyrosine (C), the band around 3426 cm^{-1} corresponds to secondary amine N—H stretching, while the band at 1621 cm^{-1} is attributed to the carbonyl (C═O) stretching vibration of the amide group. Moreover, the new band appearing at 1384 cm^{-1} is ascribed to in-plane bending vibrations of hydroxyl groups introduced by the modification (Peng et al., 2018). These spectral changes indicate the successful covalent attachment of L-tyrosine to the nanotube surface. In the final modification step, the FTIR spectrum of the MWCNT-O-L-tyrosine-p-aminobenzoic acid (D) exhibits a band at 3443 cm^{-1} corresponding to N—H stretching of primary amine groups (–NH_2), while the bands at 1630 and 1413 cm^{-1} are assigned to the C═O and C—O stretching vibrations of carboxylate groups, respectively (Gomez et al., 2019). These findings confirm the covalent bonding of the PABA molecule to the nanotube surface. Overall, the observed changes in the characteristic bands strongly support the successful stepwise functionalization of MWCNTs into MWCNT-O-L-tyrosine-p-aminobenzoic acid, with each functional group effectively integrated into the nanostructure.

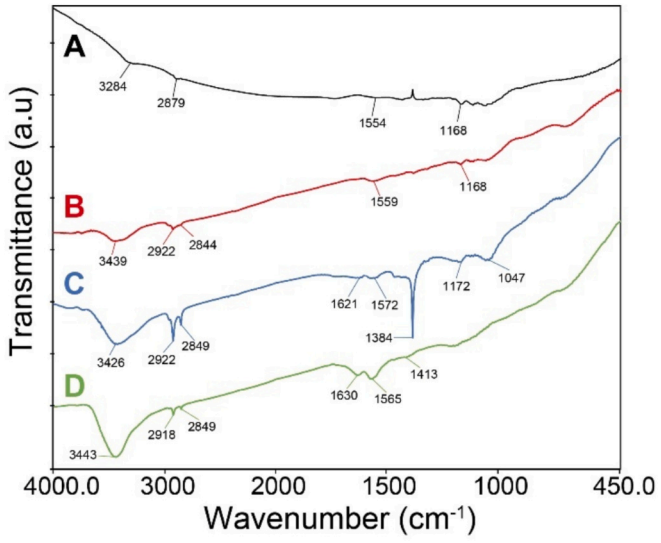

Fig. 2. FTIR spectra of MWCNT (A), MWCNT-OH (B), MWCNT-O-L-tyrosine (C), and MWCNT-O-L-tyrosine-p-aminobenzoic acid (D).

3.1.2. BET analysis

Throughout the sequential functionalization process (from A to B, B to C, and C to D), the covalent attachment of chemical groups to the MWCNT surface resulted in significant changes in the porous structure and surface characteristics of the materials. As shown in Fig. 3a, all samples exhibit type IV nitrogen adsorption-desorption isotherms with noticeable hysteresis loops, indicating a mesoporous nature (Thommes et al., 2015). However, a gradual decrease in adsorption capacity is observed from A to D, suggesting partial pore blockage due to the introduction of functional groups, which likely hinder nitrogen diffusion into the porous matrix. The BET surface area and pore volume data provided in Table 1 support these observations. While pristine MWCNTs exhibit a high surface area of 278.0 m^2/g, this value decreases sequentially to 247.6 m^2/g (MWCNT-OH), 220.3 m^2/g (MWCNT-O-L-Tyrosine), and 202.8 m^2/g (MWCNT-O-L-Tyrosine-PABA) after each modification step. Similarly, the total pore volume (Vt) decreases from 1.451 cc/g to 0.847 cc/g. These reductions clearly indicate that functional moieties occupy surface sites and partially obstruct pore entrances, thereby diminishing the accessible surface area and pore network. Fig. 3b further illustrates the changes in pore size distribution. Although all samples retain their mesoporous character, a shift toward reduced cumulative pore volume and narrower pore widths is evident after each functionalization step. This suggests that the grafted molecules preferentially occupy mesopores, contributing to the observed reduction in pore volume. In conclusion, the progressive decrease in BET surface area, pore volume, and nitrogen uptake observed in the isotherms strongly confirms the successful functionalization of MWCNTs. These structural changes are critical, as they can directly influence surface interactions, dispersion behavior, and potential performance in catalytic or biological applications.

3.1.3. SEM/EDX analysis

Fig. 4 shows the morphological images taken with SEM of pure MWCNT and MWCNT samples functionalized with various treatments. As can be clearly seen from the images, the pure MWCNT structure exhibits a highly complex, irregular, and spiral-like morphology, intertwined with each other. This structural irregularity arises as a result of the Van der Waals forces acting between the nanotubes, and these strong physical interactions cause the nanotubes to intertwine and form large aggregates. Therefore, the morphological structure observed in the SEM

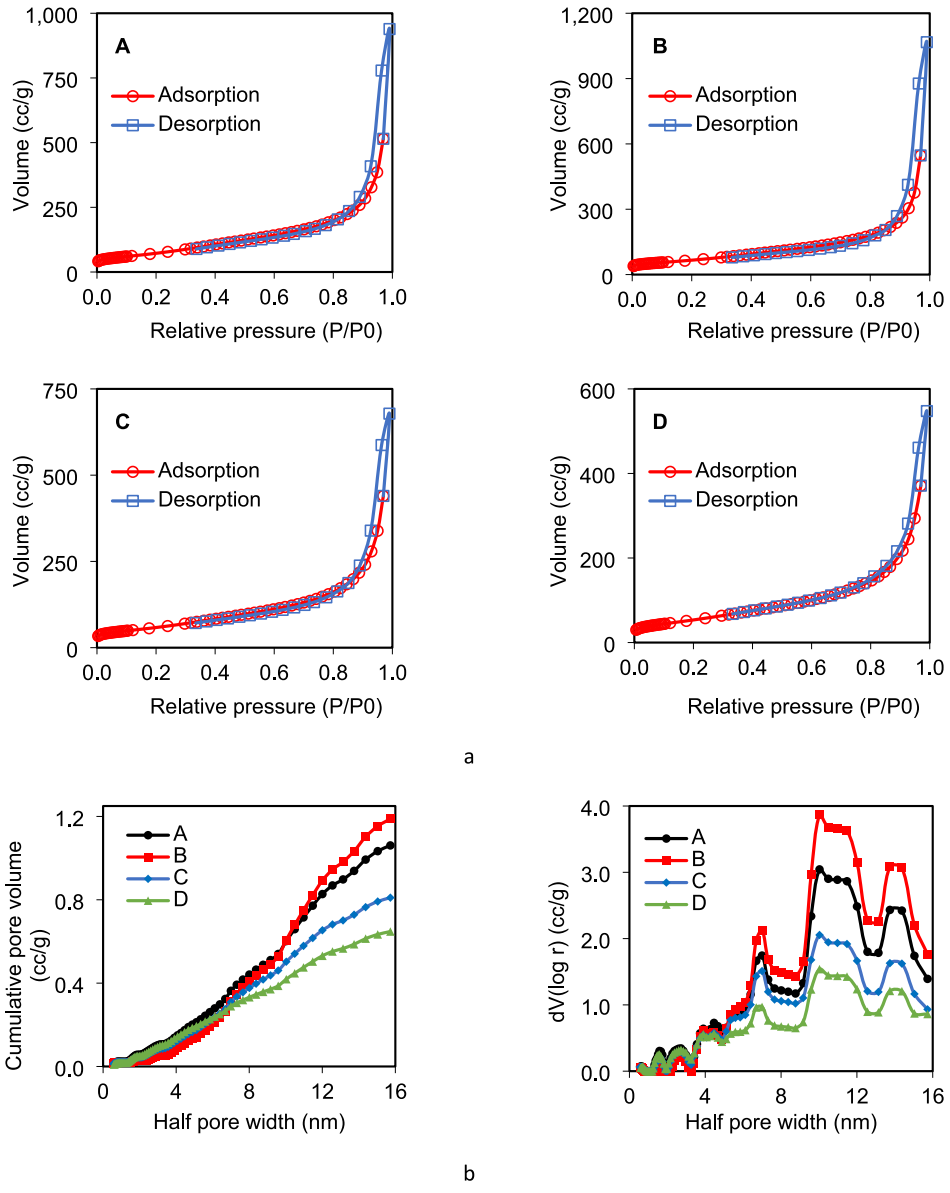

Fig. 3. a) Nitrogen adsorption–desorption isotherm curves and b) half pore width versus cumulative pore volume plots of MWCNT (A), MWCNT-OH (B), MWCNT-O-L-tyrosine (C), and MWCNT-O-L-tyrosine-p-aminobenzoic acid (D).

Table 1
BET surface areas and pore volumes of samples of MWCNT (A), MWCNT-OH (B), MWCNT-O-L-tyrosine (C), and MWCNT-O-L-tyrosine-p-aminobenzoic acid (D).

Samples	S_{BET} (m^2/g)	V_t (cc/g)	V_{mic} (cc/g)	V_{meso} (cc/g)	V_{macro} (cc/g)
MWCNT	278.0	1.451	–	1.115	0.336
MWCNT-OH	247.6	1.651	–	1.255	0.396
MWCNT-O-L-Tyrosine	220.3	1.049	–	0.846	0.203
MWCNT-O-L-Tyrosine-PABA	202.8	0.847	–	0.667	0.180

images of pure MWCNTs prevents the nanotubes from exhibiting any regular alignment. When the hydroxylated MWCNT (MWCNT-OH) sample in Fig. 4b is examined, it is striking that it has a less complex and more open structure compared to pure MWCNT. This observation supports a frequently emphasized finding in the literature. The –OH functional groups added to the nanotube surface as a result of hydroxylation weaken the Van der Waals interactions between the nanotubes, reducing their tendency to aggregation and simultaneously causing the nanotubes to mechanically shorten (Yalçınkaya et al., 2024; Kim et al., 2017). These effects result in a lower degree of aggregation and a more regular morphology. SEM images of MWCNT-O-L-tyrosine and MWCNT-O-L-tyrosine-PABA samples obtained by functionalizing MWCNTs at the same magnification (25 KX) show that L-tyrosine and then PABA molecules added to the surface further weakened the interactions between nanotubes, thus reducing aggregation. Furthermore, a shortening of the nanotubes' lengths was clearly observed as a result of the attachment of these functional groups. This reveals that functionalization significantly affects not only the chemical properties but also the morphological properties (Abdolmaleki et al., 2013; Yalçınkaya et al., 2024). It is known from the literature that MWCNTs are used in various biocatalytic applications, including dye color change and biosensing, and are versatile enzyme support materials (Azevedo, 2014; Ren et al., 2020). Fig. 4e shows an SEM image of a functionalized MWCNT with enzyme immobilization. As a result of the immobilization of the PPO enzyme onto the MWCNT surface, granular and amorphous structures were observed on the surface of the nanotubes in the SEM images,

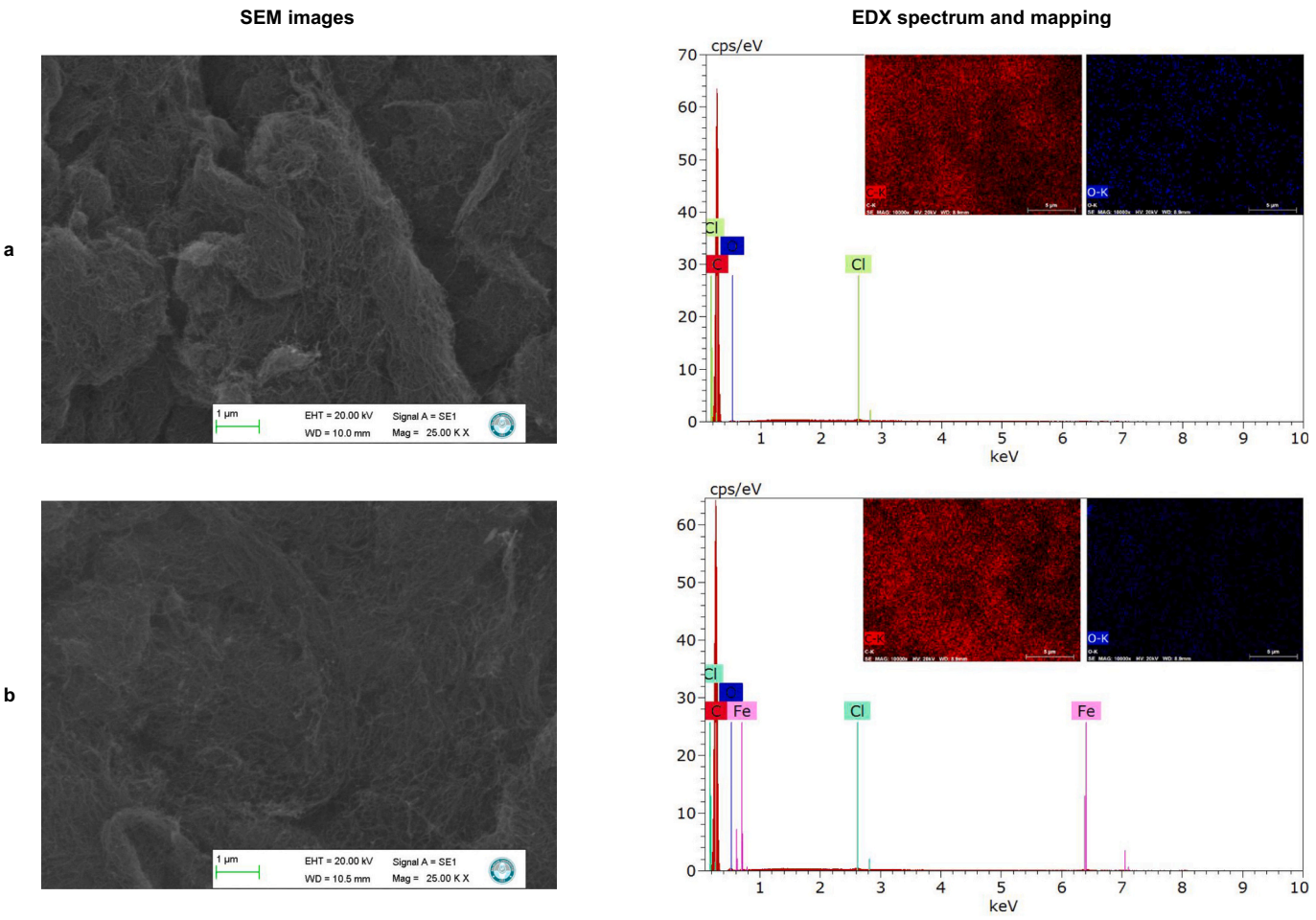

Fig. 4. SEM images, EDX spectra and elemental composition mapping of a) MWCNT (A), b) MWCNT-OH (B), c) MWCNT-O-L-tyrosine (C), d) MWCNT-O-L-tyrosine-PABA (D) and e) PPO immobilized MWCNT-O-L-tyrosine-PABA (E).

demonstrating successful attachment of the enzyme molecules to the surface. Furthermore, due to the enzyme coating, the surface of the functionalized MWCNTs became rougher, and the tendency for aggregation between the tubes increased. These morphological changes demonstrate that immobilization significantly affects the surface properties of the functionalized MWCNTs.

Fig. 4 also shows the EDX analyses of both pure and variously functionalized MWCNT samples. The weight percent elemental composition obtained from these analyses is detailed in Table 2. According to the spectral data obtained, the pure MWCNT sample contains almost all carbon, with 98.07% C element detected in this sample. In the MWCNT-OH sample subjected to hydroxylation, the carbon content decreased to 95.14%, while the oxygen content increased to 3.84%. This increase in oxygen is a direct indicator of the successful integration of hydroxyl groups into the structure. In the functionalized samples, especially in the L-tyrosine-modified sample, the nitrogen (N) element specific to the L-tyrosine structure was prominently revealed in the spectrum (0.79%). Similarly, in the sample surface-modified with PABA (para-aminobenzoic acid), a significant increase was observed in both nitrogen (N) and oxygen (O) contents. The N content was observed to increase to 1.23% and the O content to 5.39%. These findings confirm that the relevant organic molecules were successfully bound to the MWCNT structure and that the surface chemistry was changed. Trace amounts of chlorine (Cl).

were also detected in the EDX spectra. These chlorine signals are thought to originate from reagents such as hydrochloric acid (HCl) and $FeCl_2{\cdot}4H_2O$ used in the experimental procedures. Furthermore, the absence of any peaks other than carbon (C), oxygen (O), nitrogen (N), chlorine (Cl), and iron (Fe) in the EDX spectra of the pure MWCNT and functionalized MWCNT samples indicates that the samples are of high purity and do not contain any significant external contamination. Furthermore, the presence of 1.40% Na, 1.32% N, 0.41% P, 0.14% K, and 0.11% Cu in the EDX spectra of the PPO-immobilized functionalized MWCNT sample shown in Fig. 4e confirms immobilization.

3.1.4. TEM analysis

Fig. 5a and b presents the transmission electron microscopy (TEM) images of pristine multi-walled carbon nanotubes and functionalized MWCNT-O-L-tyrosine-p-aminobenzoic acid, respectively. A comparative analysis of these images reveals notable changes in the morphology and structural features of the nanotubes as a result of the functionalization process. In Fig. 5a, the pristine MWCNTs exhibit a well-defined tubular structure with smooth and clean surfaces, characteristic of untreated carbon nanotubes. The walls are distinctly visible, and there is minimal presence of surface irregularities or amorphous deposits, indicating high structural integrity and purity. Conversely, Fig. 5b, corresponding to the functionalized MWCNTs, shows a significant increase in surface roughness and the presence of an amorphous outer layer along the nanotube walls. This morphological alteration is indicative of successful surface modification through the covalent attachment of L-tyrosine and p-aminobenzoic acid functional groups. The observed coating or layer surrounding the nanotubes suggests the formation of a

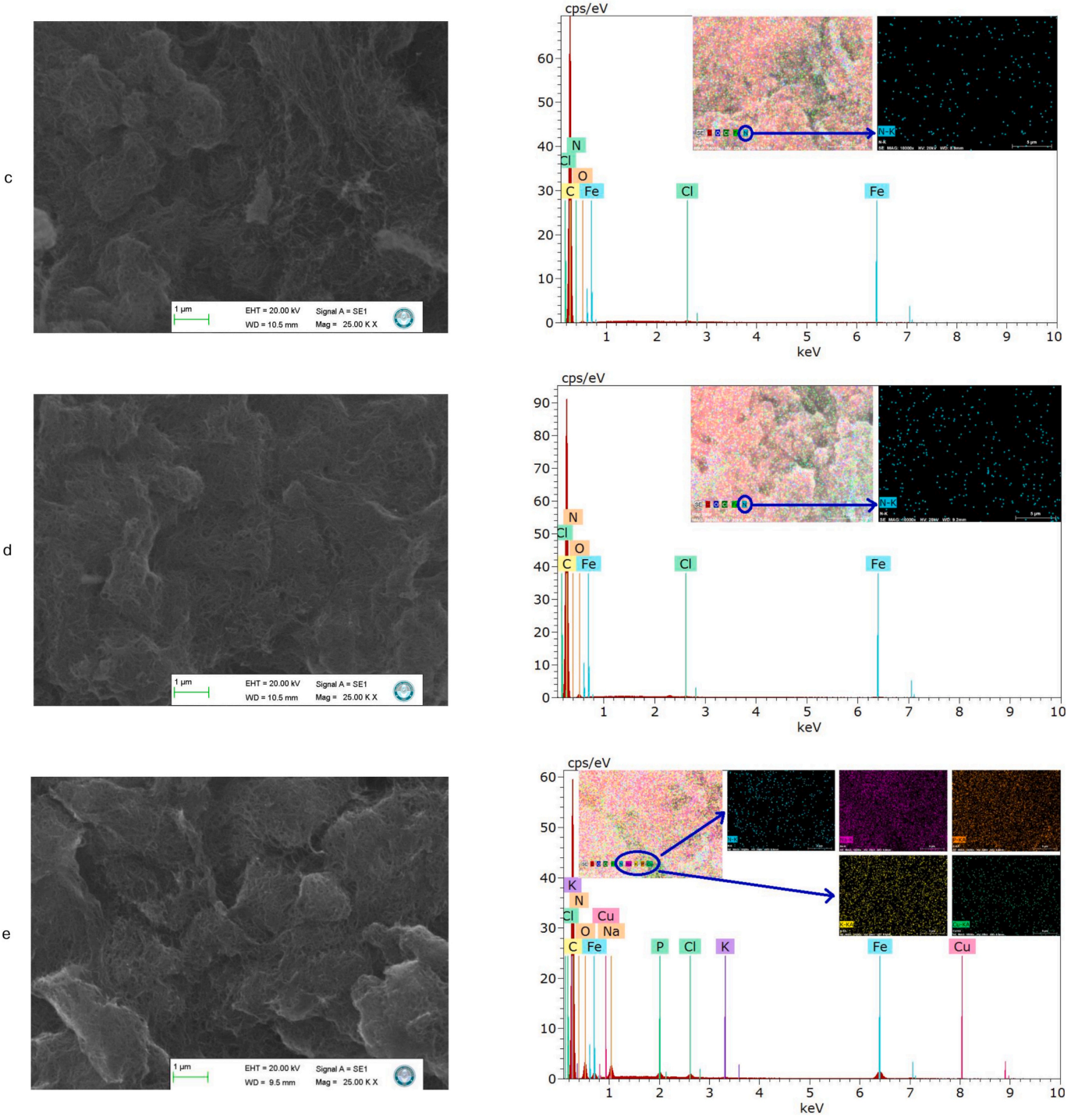

Fig. 4. (*continued*).

Table 2
Elemental composition of MWCNT, MWCNT-OH, MWCNT-O-L-tyrosine, MWCNT-O-L-tyrosine-p-aminobenzoic acid and PPO immobilized MWCNT.

Samples	C	O	Cl	Fe	N	Na	P	K	Cu
MWCNT	98.07	1.66	0.27	–	–	–	–	–	–
MWCNT-OH	95.14	3.84	0.23	0.79	–	–	–	–	–
MWCNT-O-L-Tyrosine	95.80	2.91	0.19	0.32	0.79	–	–	–	–
MWCNT-O-L-Tyrosine-PABA	92.76	5.39	0.14	0.48	1.23	–	–	–	–
PPO-MWCNT-O-L-Tyrosine-PABA	77.09	14.75	0.47	4.31	1.32	1.40	0.41	0.14	0.11

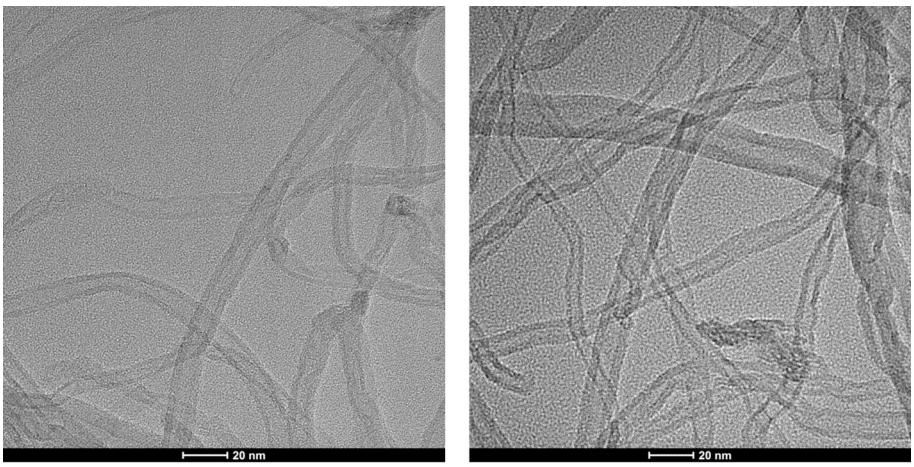

Fig. 5. TEM images of a) MWCNT and b) MWCNT-O-L-tyrosine-p-aminobenzoic acid.

uniform organic phase, which not only confirms the functionalization but also implies enhanced surface reactivity and increased number of active sites. From an application-oriented perspective, such surface modifications can considerably improve the dispersibility of MWCNTs in aqueous and polar media, enhance their biocompatibility, and provide functional groups suitable for selective biomolecular interactions or enzyme immobilization. The increased surface area and functional group density achieved through this process are particularly advantageous in affinity chromatography applications, where molecular recognition and binding specificity are critical. In summary, the TEM analysis clearly demonstrates that functionalization of MWCNTs with L-tyrosine and p-aminobenzoic acid significantly alters their surface morphology, confirming the formation of a chemically modified nanostructure with improved interfacial characteristics suitable for biotechnological applications.

3.2. Kinetic properties of PPO

Kinetic measurements were performed under the determined optimal pH and temperature conditions. Accordingly, optimal pH and temperature were established prior to kinetic analyses."

3.2.1. Optimum pH

pH is one of the key parameters affecting enzyme activity, as it directly influences the structural integrity of the enzyme and its interaction with the substrate (Sharif, 2024). Generally, enzyme activity increases with rising pH, reaches a maximum at an optimum value, and then decreases toward zero. In this context, PPO enzymes extracted from both leaf and flower tissues of *Salvia aethiopis* L. using phosphate buffer were partially purified by ammonium sulfate precipitation followed by dialysis. The optimum pH values of each obtained enzyme solution were determined using catechol, 4-methylcatechol, and pyrogallol substrates across the pH range of 4–9, in triplicate.

Fig. 6 shows pH–activity profiles for crude, ammonium sulfate–-fractionated, and dialyzed extracts obtained from leaf and flower tissues for each substrate. Examination of the graphs clearly indicates that the optimum pH values of PPO vary depending on both the substrate type and the purification stage. For enzyme solutions derived from leaf tissues, the optimum pH value for catechol was consistently determined as pH 7 at all purification stages. For 4-methylcatechol, the optimum pH was found to be pH 6 in the crude extract and pH 5 in the purified forms. In the case of pyrogallol, the optimum pH values were recorded as 9, 8, and 8, respectively, across the purification steps. Similarly, for flower-derived PPO, the optimum pH values for catechol were 7, 7, and 6; for 4-methylcatechol, 6, 6, and 5; and for pyrogallol, 8, 8, and 7, respectively. These findings demonstrate that the purification processes caused a substrate-dependent shift of PPO's optimum pH toward more acidic values. When comparing enzyme extracts from leaf and flower tissues, the general pH response trends appeared similar, suggesting that the tissue origin had no significant influence on the optimum pH values. The observed pH shifts following purification are most likely related to changes in the concentration of phenolic compounds, which are weakly acidic constituents naturally present in plant matrices. Phenolic compounds are secondary metabolites synthesized by plants, characterized by one or more hydroxyl groups attached to aromatic rings. In dilute aqueous solutions, they typically exhibit weak acidic behavior in the pH range of 5–6. The removal of certain organic components during purification might have resulted in an enzyme environment enriched in phenolic compounds, thereby shifting the PPO activity profile toward a more acidic region. The optimum pH values reported in the literature for PPO enzymes purified from various biological sources are consistent with the findings of this study. The substrate-dependent optimum pH of PPO is reported as 4.5–8.0 for catechol, 4.0–9.0 for 4-methylcatechol, and 6.5–9.0 for pyrogallol (Yıldız et al., 2022; Carvalho & Orlando, 2017; Derardja et al., 2017; Wang et al., 2021; Siddiq & Dolan, 2017; Gomes et al., 2014; Sarsenova et al., 2023; Ilesanmi et al., 2023; Benaceur et al., 2020; Karakuş et al., 2021; Faiz & Baltas, 2017; Çesko et al., 2023; Alishah et al., 2023; Demir et al., 2023; Ioniţă et al., 2017; Doğan et al., 2002, 2005, Doğan et al., 2011, Doğan et al., 2013; Doğan & Doğan, 2004; Doğan & Salman, 2007). These variations may arise from differences in enzyme source, extraction and purification methods, buffer systems, substrate types, and the cellular microlocalization of the enzymatic reaction. Therefore, the optimum pH values obtained in this study clearly demonstrate the influence of both substrate selection and purification steps on the activity profile of PPO and show strong alignment with the existing literature.

3.2.2. Optimum temperature

Temperature is a key determinant of enzymatic rate; a 10 °C increase typically doubles the reaction rate, but this trend cannot continue indefinitely because, beyond a threshold, thermal denaturation rapidly reduces activity. Consequently, each enzyme reaches maximum activity at an optimum temperature governed by its structure and biological origin; animal enzymes often show optima around 40–50 °C, whereas plant enzymes frequently exhibit higher values. In this study, the optimum temperature of PPO from *Salvia aethiopis* L. leaves and flowers was assessed at three purification stages: crude, ammonium sulfate precipitated, and dialyzed extracts. Each extract was tested at the optimum pH over 20–50 °C using catechol, 4-methylcatechol, and pyrogallol as substrates (Fig. 7).

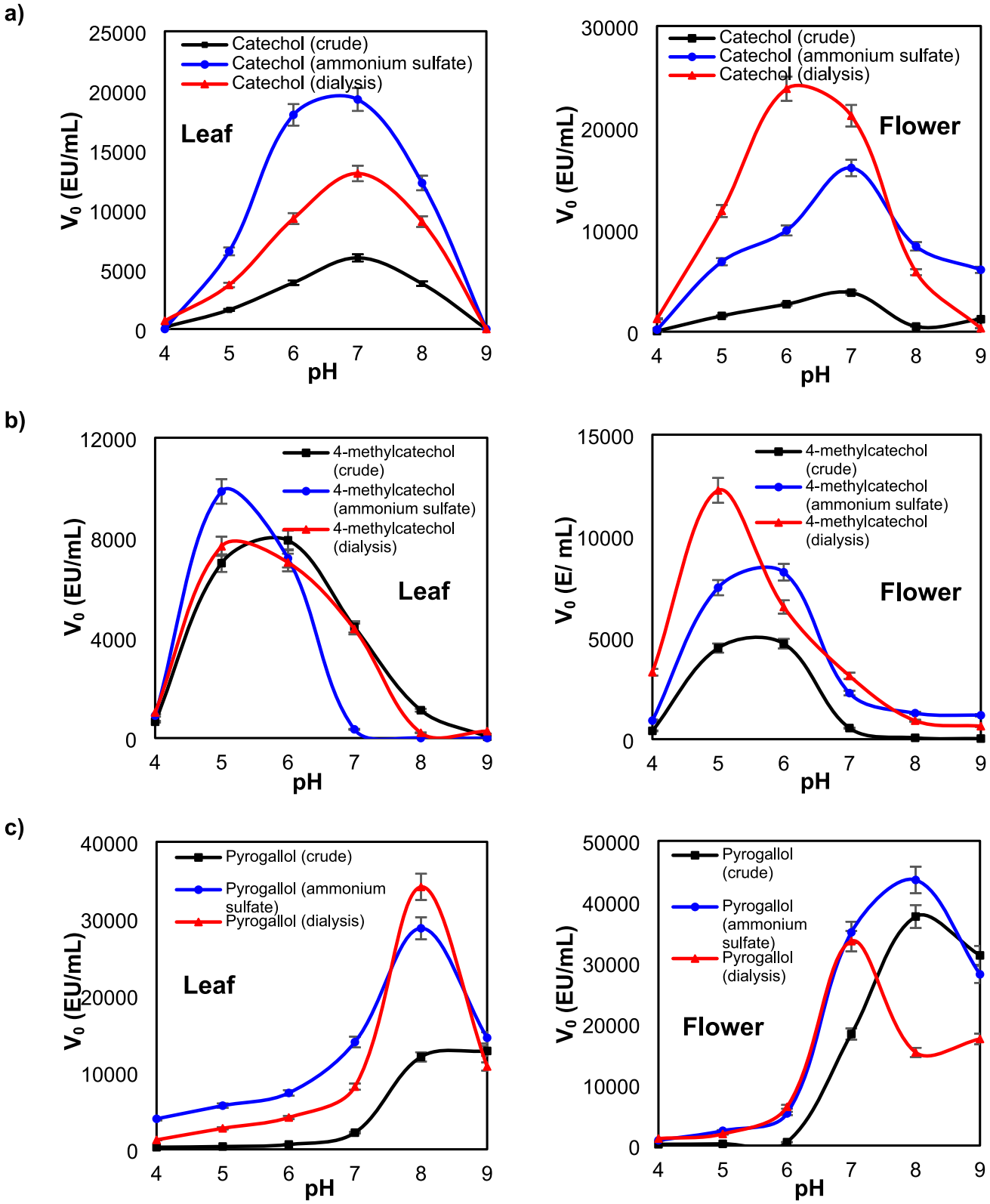

Fig. 6. pH-dependent activity profiles of PPO extracted from leaves and flowers of *Salvia aethiopis* L. for a) catechol, b) 4-methylcatechol and c) pyrogallol substrates

The data revealed that the optimum temperature of PPO enzymes from both leaf and flower sources slightly increased following purification steps. For all substrates tested, the partially purified PPO extracts obtained after ammonium sulfate precipitation and dialysis exhibited an optimum temperature of 30 °C. Beyond this temperature, a decline in enzyme activity was observed. This decrease can be attributed to the acceleration of enzyme denaturation at higher temperatures, which disrupts the active conformation of the enzyme. As a result, the active site is impaired, weakening its interaction with the substrate and reducing its catalytic efficiency. A review of the literature shows that the reported optimum temperatures for PPO enzymes from various sources span a wide range. These differences are attributed to variations in

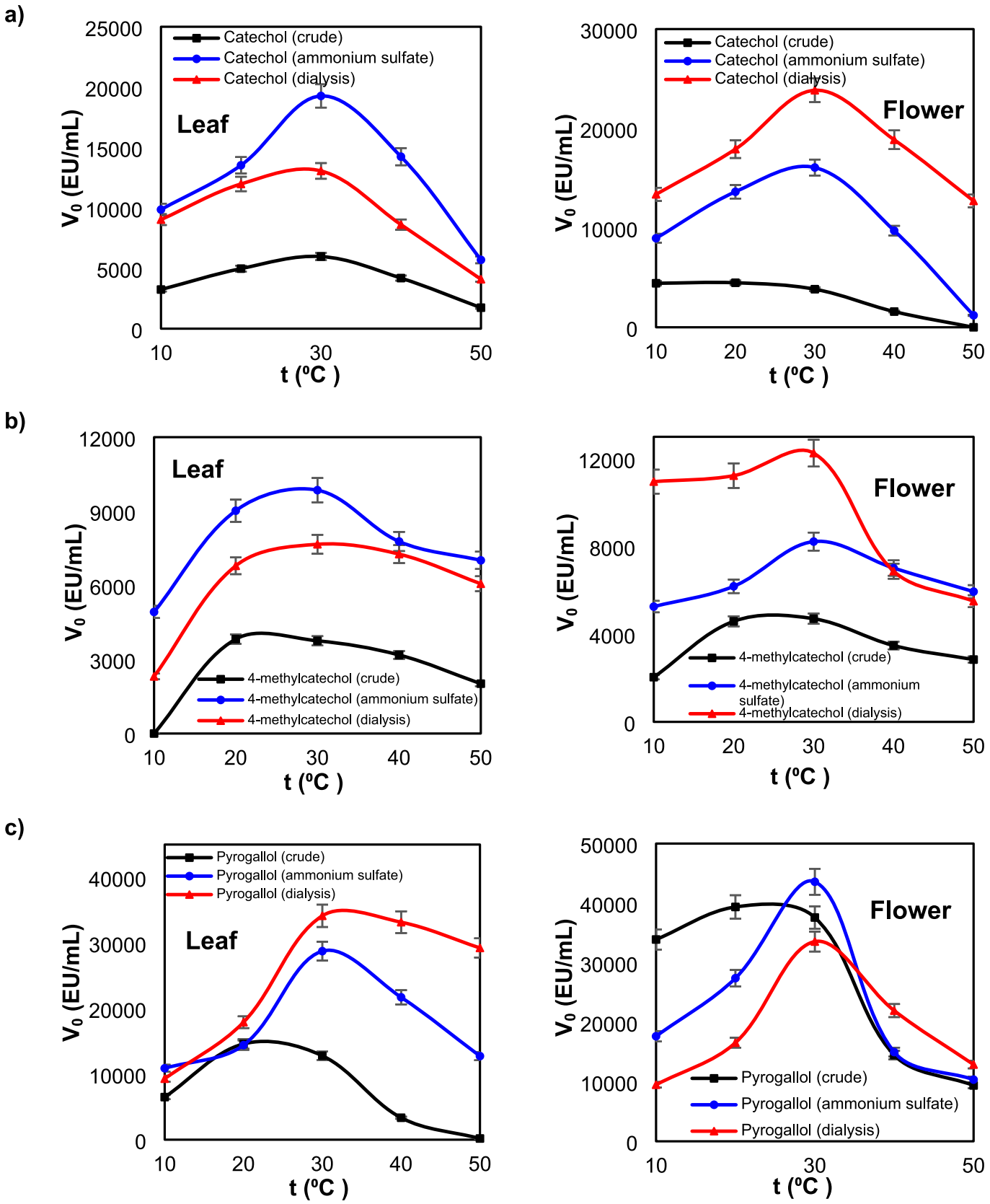

Fig. 7. Temperature-dependent activity profiles of PPO extracted from leaves and flowers of *Salvia aethiopis L.* for a) catechol, b) 4-methylcatechol and c) pyrogallol substrates.

biological origin, extraction and purification methods, and the substrate used. For example, according to the literature, the optimum temperature for PPO is substrate-dependent, ranging from 15 to 50 °C with catechol, 10–60 °C with 4-methylcatechol, and 5–60 °C with pyrogallol (Alishah et al., 2023; Benaceur et al., 2020; Carvalho & Orlando, 2017; Çesko et al., 2023; Demir et al., 2023; Derardja et al., 2017; Doğan et al., 2002, 2005; Doğan et al., 2011; Doğan et al., 2013; Doğan & Doğan, 2004; Doğan & Salman, 2007; Faiz & Baltas, 2017; Ilesanmi et al., 2023; Ioniță et al., 2017; Karakuş et al., 2021; Kaya & Bağcı, 2021; Sarsenova et al., 2023; Siddiq & Dolan, 2017; Wang et al., 2021; Yıldız et al., 2022; Zaini et al., 2013). One particularly notable observation from the literature is the reporting of extremely low optimum temperatures (~5 °C) for PPO enzymes from certain plant sources, such as avocado and damson plum, when using pyrogallol as the substrate. This indicates that some plant-derived enzymes can retain high activity even at low temperatures. The other reported values for optimum temperature fall within the expected range for plant-based PPOs. The results suggest that optimum temperature values depend not only on the purification stage of the enzyme but also on the chemical structure of the substrate and the biological origin of the enzyme. In this context, the observation that PPO from *Salvia aethiopis* L. exhibits an optimum temperature of 30 °C for all substrates regardless of purification stage indicates that the enzyme achieves maximum activity in a moderate temperature range and displays a broad substrate activity profile. This characteristic enhances the potential applicability of PPO from this species in biotechnological applications.

3.2.3. Enzyme kinetics

In this study, the kinetic parameters of PPO enzyme solutions obtained from the leaves and flowers of *Salvia aethiopis* L. were determined using catechol, 4-methylcatechol, and pyrogallol substrates at varying concentrations under previously established optimal pH and temperature conditions. The Lineweaver–Burk method was employed for enzyme kinetic calculations, from which the Michaelis-Menten constant (K_M) and the maximum reaction rate (V_{max}) were determined. To assess the substrate specificity of the enzyme, three different phenolic substrates—two diphenolic (catechol, 4-methylcatechol) and one triphenolic (pyrogallol)—were used. Measurements conducted on PPO enzyme solutions obtained from the leaf and flower parts through different purification steps (phosphate buffer extraction, ammonium sulfate precipitation, and dialysis) showed that the activity vs. concentration curves for all three substrates exhibited classical Michaelis–Menten behavior (data not shown). The data obtained from these curves were analyzed using the Lineweaver–Burk equation (Figure not shown) to calculate the K_M, V_{max}, and the catalytic efficiency (V_{max}/K_M) values, which are presented in Table 3.

For PPO extracted from leaf samples, the calculated V_{max}/K_M values for catechol were 1.43×10^6, 1.67×10^6, and 3.32×10^6; for 4-methylcatechol: 2.00×10^6, 5.01×10^6, and 3.33×10^6; and for pyrogallol: 2.00×10^7, 1.43×10^7, and 1.25×10^7, respectively, across the purification steps. These values indicate that PPO from leaf tissues exhibited the highest catalytic efficiency toward pyrogallol, suggesting that this substrate has the highest specificity. Additionally, an increase in V_{max}/K_M values for catechol and 4-methylcatechol was observed upon purification, while a slight decrease was noted for pyrogallol. A similar kinetic analysis was performed for PPO enzyme solutions obtained from flower tissues. The V_{max}/K_M values calculated for catechol were 1.67×10^6, 5.00×10^6, and 5.00×10^6; for 4-methylcatechol: 5.00×10^6, 3.33×10^6, and 1.11×10^7; and for pyrogallol: 2.50×10^7, 3.33×10^7, and 1.23×10^7, respectively. These results also clearly demonstrate that PPO extracted from the flower parts exhibited the highest specificity toward pyrogallol. Following purification, increases in the V_{max}/K_M values were observed for catechol and 4-methylcatechol, while a decreasing trend was noted for pyrogallol. In summary, both leaf- and flower-derived PPO enzymes displayed similar substrate specificity profiles, with the highest catalytic efficiency observed for pyrogallol, followed by 4-methylcatechol and catechol. Moreover, purification steps generally improved the kinetic characteristics of the enzyme solutions, notably increasing the V_{max}/K_M values, thereby enhancing the enzymes' selectivity and catalytic capacity toward substrates. These findings suggest that PPO isolated from *Salvia aethiopis* L. exhibits high specificity toward phenolic substrates and holds promising potential for various biotechnological applications.

Table 3
Kinetic parameters of the PPO enzyme.

Samples	Purification steps	Substrates	V_{max} (EU/mL)	K_M (mM)	V_{max}/K_M (EU/mL·mM)
Leaf	Crude extract	Catechol	5000	0.0035	1.430.000
		4-methylcatechol	5000	0.0025	2.000.000
		Pyrogallol	50.000	0.0025	20.000.000
	Ammonium sulfate precipitation	Catechol	142.857	0.0857	1.670.000
		4-methylcatechol	16.667	0.00333	5.010.000
		Pyrogallol	25.000	0.00175	14.300.000
	Dialysis	Catechol	14.286	0.0043	3.320.000
		4-methylcatechol	10.000	0.0030	3.330.000
		Pyrogallol	5000	0.0040	12.500.00
Flower	Crude extract	Catechol	5000	0.0030	1.670.000
		4-methylcatechol	10.000	0.0020	5.000.000
		Pyrogallol	50.000	0.0020	25.000.000
	Ammonium sulfate precipitation	Catechol	12.500	0.0025	5.000.000
		4-methylcatechol	10.000	0.0030	3.330.000
		Pyrogallol	25.000	0.00075	33.300.000
	Dialysis	Catechol	25.000	0.0050	5.000.000
		4-methylcatechol	14.286	0.00129	11.100.000
		Pyrogallol	33.333	0.0027	12.300.000

3.3. Enzyme purification

The PPO enzyme extracted from *Salvia aethiopis* L., *Salvia officinalis* L. and mushroom was purified through successive steps including ammonium sulfate precipitation, dialysis, and affinity chromatography. For each purification step, enzyme activity (EU/mL) and protein concentration (mg/mL) were determined, and these values were used to calculate specific activity (EU/mg protein) and purification fold. The quantitative results of the purification process are summarized in Table 4. Upon analysis of the data, it is evident that the purification efficiency of PPO differs depending on whether it is derived from leaf or flower tissues. The PPO enzyme isolated from leaf extracts achieved an 8.4-fold purification compared to the crude extract, representing the highest purification yield among all tested methods. Notably, this success was achieved in the affinity chromatography step, reaching an enzyme activity of 5721 EU/mL and a specific activity of 5371 EU/mg protein. These results clearly demonstrate the high selectivity and efficiency of the carbon nanotube-based functional affinity matrix in purifying leaf-derived PPO. When the same purification steps were applied to flower-derived PPO, a total of 3-fold purification was achieved, with the highest specific activity (5576 EU/mg protein) again obtained via affinity chromatography. However, compared to the leaf-derived enzyme, the overall purification efficiency for flower-derived PPO was lower. This discrepancy may be attributed to differences in the composition of phenolic compounds and their interactions with the enzyme in leaf and flower tissues. In particular, the removal of low-molecular-weight phenolic compounds from leaf extracts during dialysis through membrane pores may have facilitated the acquisition of a more purified enzyme solution. Alternatively, the differences in protein migration rates through the affinity column could have allowed for more efficient separation of the enzyme in the leaf extract. Moreover, it is noteworthy

Table 4
Purification data of PPO enzyme with different techniques.

Plants	Enzyme sources	Purification steps	Enzyme activity (EU/mL)	Amount of protein (mg/mL)	Specific activity (EU/mg)	Purification ratio
Salvia aethiopis L.	Leaf	Crude extract	1139	1.779	640	–
		Ammonium sulfate precipitation	1572	2.023	777	1.2
		Dialysis	4320	1.218	3546	5.5
		Affinity chromatography	5721	1.065	5371	8.4
	Flower	Crude extract	1849	0.839	1849	–
		Ammonium sulfate precipitation	2073	1.067	1942	1.1
		Dialysis	2212	1.042	2122	1.2
		Affinity chromatography	619	0.111	5576	3
Salvia officinalis L.	Leaf	Crude extract	614	1.101	558	–
		Ammonium sulfate precipitation	4847	1.120	4327	7.8
		Dialysis	7298	1.205	6056	10.9
		Affinity chromatography	11,234	1.230	9133	16.4
Mushroom	–	Crude extract	1034	0.290	3565	–
		Ammonium sulfate precipitation	6364	0.306	20,797	5.8
		Dialysis	9500	0.312	30,449	8.54
		Affinity chromatography	14,934	0.324	46,092	12.9

that among all purification steps, affinity chromatography yielded the highest purification fold for both leaf- and flower-derived PPO. The effective elution of PPO upon increasing the pH from 5.0 to 7.0 confirms that the enzyme–matrix interaction is governed by reversible affinity forces, and that enzyme release is achieved through a deliberate reduction in interaction strength under mild conditions. This finding highlights the effectiveness of the functional carbon nanotube-based affinity matrix synthesized in this study, outperforming conventional purification methods in isolating PPO. Nonetheless, the results also indicate that achieving highly pure enzyme preparations may not be solely feasible using this matrix alone, and that more advanced or combined purification strategies may be required. In addition to *Salvia aethiopis* L., the functional affinity matrix was further evaluated using *Salvia officinalis* L. leaf PPO to assess its selectivity and reusability. Remarkably, the affinity chromatography step yielded a purification fold of 16.4 for *S. officinalis* L. PPO, which is approximately twice the enrichment obtained for *S. aethiopis* L. leaf extracts (8.4-fold). This high purification fold was accompanied by a specific activity of 9133 EU/mg and an enzyme activity of 11,234 EU/mL, demonstrating that the matrix performs even more efficiently with *S. officinalis* L. PPO. These findings confirm that the synthesized MWCNT-based affinity matrix is capable of selectively capturing PPO from different botanical sources with high efficiency, and its performance is not restricted to a single plant species.

In addition to plant-derived PPOs, the purification performance of the affinity matrix was also evaluated using mushroom-derived PPO, a widely accepted model enzyme for enzymatic browning studies. The mushroom PPO exhibited a clear enrichment after affinity chromatography, with a notable increase in specific activity compared to the crude extract, confirming the effective interaction between the enzyme and the functionalized MWCNT-based matrix (Table 4). The successful purification of mushroom PPO further demonstrates that the affinity matrix is not limited to plant tissues but can also efficiently capture PPO from fungal sources, reinforcing its broad applicability and robustness.

To contextualize the performance of the developed matrix, we benchmarked our purification fold against the reports using Sephadex G-100, ion-exchange chromatography, and Sepharose 4B–based affinity supports. Across these studies, some reported purification folds range from 2.70 to 13.90 (ion-exchange chromatography: ~2.70–3.32; Sephadex G-100–6.50–11.05; Sepharose 4B affinity: ~9.02–13.90) (Erat et al., 2006; Ünal et al., 2011; Guo et al., 2009; Ilesanmi et al., 2023; Yu et al., 2024; Oz et al., 2013; Aksoy, 2020; Öztürk & Küfrevioğlu, 2024; Doğan et al., 2005). For *Salvia aethiopis* L., our result (8.40-fold) falls squarely within this range: it exceeds typical ion-exchange outcomes, is comparable to Sephadex G-100, and approaches the performance of Sepharose 4B–based affinity systems, **while enabling reuse under mild conditions and supporting cost-effective scale-up**. Importantly, the 16.4-fold purification obtained for *S. officinalis* L. PPO surpasses the upper limit of many conventional systems, positioning the MWCNT-based matrix as a highly competitive alternative to traditional affinity supports such as Sepharose 4B. This superior enrichment further validates the functional group design and ligand architecture of the synthesized matrix. The selective capture of PPO by the functionalized MWCNT matrix can be rationalized as follows: aromatic residues engage in π–π stacking with the graphitic surface, augmented by van der Waals/hydrophobic contacts; carboxyl/amine groups introduced during functionalization contribute electrostatic and hydrogen-bonding interactions that stabilize adsorption and favor specific orientations. These effects are well documented for proteins on CNTs and are strengthened when nanotube surface chemistry is tailored. In our design, L-tyrosine acts as a spacer to project the recognition element from the support, while p-aminobenzoic acid (PABA) functions as an inhibitor-mimetic ligand for PPO/tyrosinase, thereby increasing binding selectivity under mild conditions; together, these features explain the observed enrichment without harsh elution (Zhang et al., 2019; Kumari et al., 2021; Rezazade et al., 2024). Beyond the purification fold, we also evaluated recovery: in leaf fractions, the affinity step increased specific activity by ~1.5× and activity density by ~1.3×, indicating selectivity gains without sacrificing overall activity; in flower fractions, specific activity rose by ~2.6× while activity density decreased, retaining ≈28% of the starting value. This divergence likely reflects tissue-specific isoenzyme distributions and the phenolic milieu, and suggests that elution stringency (pH/ionic strength/competitive ligand) can be tuned to improve recovery without compromising selectivity; with complete volume/activity records, these trends can be converted to true percentage yields in future runs. From a process standpoint, the functionalized MWCNT support is cost-effective for scale-up because its high specific surface area enables target capacity with smaller bed volumes (lower resin/buffer use), its mechanical/chemical robustness supports regeneration and reuse with limited capacity loss, and its tunable surface chemistry permits selective binding under milder conditions, shortening processing time and minimizing activity loss. Taken together, the MWCNT matrix couples literature-level enrichment with adjustable recovery and favorable cost drivers, underscoring both its novelty and operational advantage over existing PPO purification protocols. The strong performance observed for both *S. aethiopis* L. and *S. officinalis* L. confirms that the matrix is robust, versatile, and broadly compatible

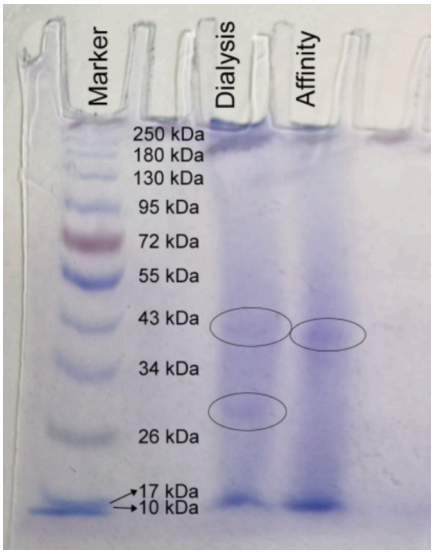

Fig. 8. SDS-PAGE electrophoresis for *Salvia officinalis* L. PPO

with PPOs from different botanical sources.

Furthermore, SDS-PAGE analysis (Fig. 8) revealed a marked simplification of the protein profile of *Salvia officinalis* L. PPO throughout the purification steps. In the dialysis fraction, two distinct bands appearing at approximately 43–45 kDa and 28–32 kDa indicated that the sample still contained multiple protein components or possible PPO isoforms at this stage. In contrast, the affinity chromatography fraction exhibited a single band around 43–45 kDa, with the double-band pattern completely eliminated. This outcome demonstrates that the functionalized MWCNT-based affinity matrix exhibits high selectivity, capturing only a single molecular form of PPO while effectively removing other proteins or isoforms that contribute to sample heterogeneity. Overall, the SDS-PAGE profile clearly shows that dialysis provides only limited purification, whereas affinity chromatography successfully isolates PPO in a single molecular form, achieving a high level of purity. These findings confirm that the developed functionalized MWCNT-based affinity matrix is a highly selective and efficient platform for PPO purification.

4. Conclusions

This study demonstrates that functionalized multi-walled carbon nanotubes modified with L-tyrosine and p-aminobenzoic acid provide an effective and highly selective affinity platform for the purification of polyphenol oxidase from *Salvia aethiopis* L., *Salvia officinalis* L. and mushroom. The designed matrix yielded an 8.4-fold purification for *S. aethiopis* L. leaf extracts and 3-fold for flower extracts, confirming its strong selectivity toward leaf-derived enzyme. Importantly, when the same affinity matrix was applied to *S. officinalis* L., a substantially higher purification fold of 16.4 was achieved, indicating that the matrix exhibits broad applicability and potentially even greater affinity toward PPO sources enriched in phenolic substrates. For mushroom-derived PPO, the affinity chromatography step resulted in a purification fold of 12.9, demonstrating the high efficiency of the functionalized MWCNT-based affinity matrix in enriching PPO from fungal sources.

Structural characterization (FTIR, BET, SEM/EDX, TEM) confirmed successful stepwise functionalization of the MWCNT surface. The BET surface area decreased from 278.0 to 202.8 $m^2 \bullet g^{-1}$ and total pore volume from 1.451 to 0.847 $cm^3 \bullet g^{-1}$ following ligand grafting, consistent with partial pore blocking and effective surface modification. Kinetic analyses revealed that the catalytic efficiency (V_{max}/K_M) followed the general order pyrogallol >4-methylcatechol > catechol, and that optimum pH and temperature varied depending on both substrate and purification level, underscoring the sensitivity of PPO catalysis to microenvironmental conditions.

SDS-PAGE analyses further validated purification outcomes. For *S. officinalis* L., the dialysis fraction displayed two bands (≈43–45 kDa and 28–32 kDa), whereas affinity chromatography produced a single sharp band at ≈43–45 kDa, demonstrating that the functionalized MWCNT matrix selectively isolated a single PPO form while efficiently removing other protein impurities or isoforms.

Overall, these results confirm that *S. aethiopis* L. and *S. officinalis* L. are valuable botanical sources of PPO, and that functionalized carbon nanotube-based affinity platforms represent a powerful tool for enzyme purification in biotechnological, food, and analytical applications. The observed purification efficiencies—especially the 16.4-fold enrichment in *S. officinalis* L. leaf PPO—highlight the matrix's robustness and broad utility. In addition, the successful purification of mushroom-derived PPO with a purification fold of 12.9 further demonstrates that the affinity matrix is equally effective for fungal PPOs, which are widely used as model enzymes in enzymatic browning studies. This result confirms that the applicability of the developed MWCNT-based affinity platform is not limited to plant sources but extends to different biological origins of PPO. As the purpose of this study was to establish the feasibility of a functionalized MWCNT-based affinity support, the demonstrated purification folds fall within or exceed typical ranges reported for plant PPOs. Further process optimization is expected to enhance both yield and purity, positioning this system as a promising next-generation platform for nanomaterial-assisted enzyme purification.

CRediT authorship contribution statement

Mehmet Doğan: Writing – review & editing, Writing – original draft, Visualization, Validation, Supervision, Software, Project administration, Methodology, Formal analysis, Data curation, Conceptualization. **Fatma Nur Yalçinkaya:** Validation, Software, Resources, Methodology, Investigation. **Zeynep Bicil:** Writing – original draft, Validation, Supervision, Software, Resources, Methodology, Investigation, Data curation. **Berna Koçer Kizilduman:** Writing – original draft, Validation, Software, Methodology, Investigation, Formal analysis, Data curation. **Serap Doğan:** Writing – original draft, Validation, Methodology.

Declaration of competing interest

The authors declare the following financial interests/personal relationships which may be considered as potential competing interests: This work was supported by TUBITAK (Project Number: 122Z634).

Acknowledgment

This work was supported by TUBITAK (Project Number: 122Z634).

Data availability

Data will be made available on request.

References

Abdolmaleki, A., Mallakpour, S., & Borandeh, S. (2013). Amino acid-functionalized multi-walled carbon nanotubes for improving compatibility with chiral poly(amide-ester-imide) containing l-phenylalanine and l-tyrosine linkages. *Applied Surface Science, 287*, 117–123. https://doi.org/10.1016/j.apsusc.2013.09.088

Aksoy, M. (2020). A new insight into purification of polyphenol oxidase and inhibition effect of curcumin and quercetin on potato polyphenol oxidase. *Protein Expression and Purification, 171*, Article 105612. https://doi.org/10.1016/j.pep.2020.105612

Alishah, M. M., Yıldız, S., Bilen, Ç., & Karakuş, E. (2023). Purification and characterization of avocado (*Persea americana*) polyphenol oxidase by affinity chromatography. *Preparative Biochemistry & Biotechnology, 53*(1), 40–53. https://doi.org/10.1080/10826068.2022.2035747

Arslan, O., Erzengin, M., Sinan, S., & Özensoy, O. (2004). Purification of mulberry (*Morus alba* L.) polyphenol oxidase by affinity chromatography and investigation of its kinetic and electrophoretic properties. *Food Chemistry, 88*(3), 479–484. https://doi.org/10.1016/j.foodchem.2004.04.005

Azevedo, R. A. M. (2014). *Immobilization of peroxidase on functionalized carbon nanotubes for synthesis of biocatalysts with high performance*. Master's thesis, University of Porto, Portugal.

Benaceur, F., Chaibi, R., Berrabah, F., Neifar, A., Leboukh, M., Benaceur, K., et al. (2020). Purification and characterization of latent polyphenol oxidase from truffles (*Terfezia arenaria*). *International Journal of Biological Macromolecules, 145*, 885–893. https://doi.org/10.1016/j.ijbiomac.2019.09.126

Bicil, Z. (2026). Adsorption kinetics and mechanism of hydrogen on pristine and functionalized multi-walled carbon nanotubes. *Fuel, 403*, Article 136130. https://doi.org/10.1016/j.fuel.2025.136130

Bradford, M. (1976). A rapid and sensitive method for the quantification of microgram quantities of protein utilizing the principle of protein-dye binding. *Analytical Biochemistry, 72*, 248–254. https://doi.org/10.1016/0003-2697(76)90527-3

Çakır, Ü., Kestel, F., Koçer Kızılduman, B., Bicil, Z., & Doğan, M. (2021). Multi-walled carbon nanotubes functionalized by hydroxyl and Schiff base and their hydrogen storage properties. *Diamond and Related Materials, 120*, Article 108604. https://doi.org/10.1016/j.diamond.2021.108604

Çam, Ş., Doğan, M., Beyli, P. T., Doğan, S., Bicil, Z., & Kızılduman, B. K. (2025). Immobilization, optimization, characterization and kinetic properties of polyphenol oxidase to multi-walled carbon nanotube. *Preparative Biochemistry & Biotechnology, 1–14*. https://doi.org/10.1080/10826068.2025.2498460

Carvalho, J. O., & Orlando, J. F. F. (2017). Heat stability and effect of pH on enzyme activity of polyphenol oxidase in *Buriti* (*Mauritia flexuosa* Linnaeus f.) fruit extract. *Food Chemistry, 233*, 159–163. https://doi.org/10.1016/j.foodchem.2017.04.145

Çatak, E., & Atalay, A. (2022). Economic and medical values of the Lamiaceae (Labiatae) (Ballıbabagiller) family. *Euroasia Journal of Mathematics, Engineering, Natural & Medical Sciences, 9*(20). https://doi.org/10.38065/euroasiaorg.941

Çesko, C., Gashi, S., Arabacı, G., Palüzar, H., Durmishi, B., Bruçi, E., et al. (2023). Investigation of the effects of pesticides on 'Jonagold' apple (*Malus* × *domestica*) polyphenol oxidase enzyme activity. *Turkish Journal of Agriculture and Forestry, 47*(1), 7. https://doi.org/10.55730/1300-011X.3064

Chazarra, S., Garcıa-Carmona, F., & Cabanes, J. (2001). Evidence for a tetrameric form of iceberg lettuce (*Lactuca sativa* L.) polyphenol oxidase: Purification and characterization. *Journal of Agricultural and Food Chemistry, 49*, 4870–4875. https://doi.org/10.1021/jf0100301

Demir, D., Kabak, S., & Çağlayan, K. (2023). Purification and characterization of polyphenol oxidase in the fruits of *Opuntia ficus-indica*. *Biology, 12*(10), 1339. https://doi.org/10.3390/biology12101339

Derardja, A. E., Pretzler, M., Kampatsikas, I., Barkat, M., & Rompel, A. (2017). Purification and characterization of latent polyphenol oxidase from apricot (*Prunus armeniaca* L.). *Journal of Agricultural and Food Chemistry, 65*(37), 8203–8212. https://doi.org/10.1021/acs.jafc.7b03210

Doğan, M., Arslan, O., & Doğan, S. (2002). Substrate specificity, heat inactivation and inhibition of polyphenol oxidase from different aubergine cultivars. *International Journal of Food Science and Technology, 37*, 415–423. https://doi.org/10.1046/j.1365-2621.2002.00580.x

Doğan, S., Ayyıldız, Y., Doğan, M., Alan, Ü., & Diken, M. E. (2013). Characterisation of polyphenol oxidase from *Melissa officinalis* L. subsp. *officinalis* (lemon balm). *Czech Journal of Food Sciences, 31*(2), 156–165. https://doi.org/10.17221/288/2011-CJFS

Doğan, S., Diken, M. E., Turhan, Y., Alan, Ü., Doğan, M., & Alkan, M. (2011). Characterization and inhibition of *Rosmarinus officinalis* L. polyphenol oxidase. *European Food Research and Technology, 233*, 293–301. https://doi.org/10.1007/s00217-011-1504-y

Doğan, S., & Doğan, M. (2004). Determination of kinetic properties of polyphenol oxidase from *Thymus* (*Thymus longicaulis* subsp. *chaubardii* var. *chaubardii*). *Food Chemistry, 88*(1), 69–77. https://doi.org/10.1016/j.foodchem.2003.12.025

Doğan, S., & Salman, Ü. (2007). Partial characterization of lettuce (*Lactuca sativa* L.) polyphenol oxidase. *European Food Research and Technology, 226*, 93–103. https://doi.org/10.1007/s00217-006-0513-8

Doğan, S., Turan, P., & Doğan, M. (2006). Some kinetic properties of polyphenol oxidase from *Thymbra spicata* L. var. *spicata*. *Process Biochemistry, 41*(12), 2379–2385. https://doi.org/10.1016/j.procbio.2006.06.013

Doğan, S., Turan, P., Doğan, M., Alkan, M., & Arslan, O. (2007). Inhibition kinetics of polyphenol oxidase by glutamic acid. *European Food Research and Technology, 225*, 67–73. https://doi.org/10.1007/s00217-006-0383-0

Doğan, S., Turan, P., Doğan, M., Alkan, M., & Arslan, O. (2008). Inhibition kinetics and mechanism of polyphenol oxidase from various sources by diethyldithiocarbamic acid. *International Journal of Food Science and Technology, 43*, 1316–1322. https://doi.org/10.1111/j.1365-2621.2007.01610.x

Doğan, S., Turan, P., Doğan, M., Arslan, O., & Alkan, M. (2005). Purification and characterization of *Ocimum basilicum* L. polyphenol oxidase. *Journal of Agricultural and Food Chemistry, 53*(26), 10224–10230. https://doi.org/10.1021/jf051646j

Dorman, H. J. D., Bachmayer, O., Kosar, M., & Hiltunen, R. (2004). Antioxidant properties of aqueous extracts from selected *Lamiaceae* species grown in Turkey. *Journal of Agricultural and Food Chemistry, 52*, 762–770. https://doi.org/10.1021/jf034908v

Dubey, R., Dutta, D., Sarkar, A., & Chattopadhyay, P. (2021). Functionalized carbon nanotubes: Synthesis, properties and applications in water purification, drug delivery, and material and biomedical sciences. *Nanoscale Advances, 3*, 5722–5736. https://doi.org/10.1039/d1na00293g

Erat, M., Sakiroglu, H., & Küfrevioğlu, Ö.İ. (2006). Purification and characterization of polyphenol oxidase from Ferula sp. *Food Chemistry, 95*(3), 503–508. https://doi.org/10.1016/j.foodchem.2005.01.044

Faiz, Ö., & Baltas, N. (2017). Polyphenol oxidase properties, anti-urease, and anti-acetylcholinesterase activity of *Diospyros lotus* L. (plum persimmon). *International Journal of Food Properties, 20*(5), 1186–1196. https://doi.org/10.1080/10942912.2016.1205086

Gao, T., Yu, J., Zhou, Y., & Jiang, X. (2017). Performance of xanthate-modified multi-walled carbon nanotubes on adsorption of lead ions. *Water, Air, & Soil Pollution, 228*(5), 172. https://doi.org/10.1007/s11270-017-3359-8

Gomes, M. H., Vieira, T., Fundo, J. F., & Almeida, D. P. F. (2014). Polyphenoloxidase activity and browning in fresh-cut 'Rocha' pear as affected by pH, phenolic substrates, and antibrowning additives. *Postharvest Biology and Technology, 91*, 32–38. https://doi.org/10.1016/j.postharvbio.2013.12.013

Gomez, N. A. G., Maruyama, S. A., Leuteritz, A., & Wypych, F. (2019). Composites of polyethylene and layered cobalt hydroxide salts as potential ultraviolet radiation absorbers. *Polymer Bulletin, 77*, 255–273. https://doi.org/10.1007/s00289-019-02742-x

Guo, L., Ma, Y., Shi, J., & Xue, S. (2009). The purification and characterization of polyphenol oxidase from green bean (*Phaseolus vulgaris* L.). *Food Chemistry, 117*(1), 143–151. https://doi.org/10.1016/j.foodchem.2009.03.088

Hussein, M. A., El-Shishtawy, R. M., Alamry, K. A., Asiri, A. M., & Mohamed, S. A. (2019). Efficient water disinfection using hybrid polyaniline/graphene/carbon nanotube nanocomposites. *Environmental Technology, 40*(21), 2813–2824. https://doi.org/10.1080/09593330.2018.1466921

Ilesanmi, O. S., Adedugbe, O. F., Oyegoke, D. A., Adebayo, R. F., & Agboola, E. (2023). Biochemical properties of purified polyphenol oxidase from bitter leaf (*Vernonia amygdalina*). *Heliyon, 9*(6), Article e17365. https://doi.org/10.1016/j.heliyon.2023.e17365

Ioniță, E., Gurgu, L., Aprodu, I., Stănciuc, N., Dalmadi, I., Bahrim, G., et al. (2017). Characterization, purification, and temperature/pressure stability of polyphenol oxidase extracted from plums (*Prunus domestica*). *Process Biochemistry, 56*, 177–185. https://doi.org/10.1016/j.procbio.2017.02.014

Karakuş, Y. Y., Yıldırım, B., & Acemi, A. (2021). Characterization of polyphenol oxidase from fennel (*Foeniculum vulgare* mill.) seeds as a promising source. *International Journal of Biological Macromolecules, 170*, 261–271. https://doi.org/10.1016/j.ijbiomac.2020.12.147

Kaya, E. D., & Bağcı, O. (2021). Purification and biochemical characterization of polyphenol oxidase extracted from Kirmizi Kismis grape (*Vitis vinifera* L.). *Journal of Food Biochemistry, 45*(8), Article e13627. https://doi.org/10.1111/jfbc.13627

Kim, M.-U., Lee, J.-M., Roh, H.-G., Kang, H.-J., Park, S.-H., Oh, S.-J., Lee, J.-S., & Park, J.-S. (2017). Covalent functionalization of multi-walled carbon nanotubes surface via chemical treatment. *Journal of Nanoscience and Nanotechnology, 17*(4), 2463–2470. https://doi.org/10.1166/jnn.2017.13311

Kumari, A., Rajeev, R., Benny, L., Sudhakar, Y. N., Varghese, A., & Hegde, G. (2021). Recent advances in carbon nanotubes-based biocatalysts and their applications. *Advances in Colloid and Interface Science, 297*, Article 102542. https://doi.org/10.1016/j.cis.2021.102542

Kürkcüoğlu, M., Tumen, G., & Baser, K. H. C. (2001). Essential oil constituents of *Satureja boissieri* from Turkey. *Chemistry of Natural Compounds, 37*, 329–331. https://doi.org/10.1023/A:1013714316862

Ma, Y., Ma, Y., Wang, S., Zhai, Y., Xiang, Q., & Li, X. (2025). Elucidating the inhibitory activity and mechanism of ergothioneine on polyphenol oxidase from mushroom. International journal of biological macromolecules. *International Journal of Biological Macromolecules, 328*(2), Article 147752. https://doi.org/10.1016/j.ijbiomac.2025.147752

Mohammadi, A., Moghaddam, A. B., Dinarvand, R., & Rezaei-Zarchi, S. (2009). Direct electron transfer of polyphenol oxidase on carbon nanotube surfaces: Application in biosensing. *International Journal of Electrochemical Science, 4*(7), 895–905. https://doi.org/10.1016/S1452-3981(23)15193-5

Ombaka, L. M., Ndungu, P. G., & Nyamori, V. O. (2014). Pyrrolic nitrogen-doped carbon nanotubes: Physicochemical properties, interactions with Pd and their role in the selective hydrogenation of nitrobenzophenone. *RSC Advances, 5*, 109–122. https://doi.org/10.1039/C4RA12523A

Oskin, P., Demkina, I., Dmitrieva, E., & Alferov, S. (2023). Functionalization of carbon nanotubes surface by aryl groups: A review. *Nanomaterials, 13*, Article 1630. https://doi.org/10.3390/nano13101630

Oyetade, O. A., Nyamori, V. O., Martincigh, B. S., & Jonnalagadda, S. B. (2015). Effectiveness of carbon nanotube-cobalt ferrite nanocomposites for the adsorption of rhodamine B from aqueous solutions. *RSC Advances, 5*, 22724–22739. https://doi.org/10.1039/C4RA15446K

Oz, F., Colak, A., Ozel, A., Ertunga, N. S., & Sesli, E. (2013). Purification and characterization of a mushroom polyphenol oxidase and its activity in organic solvents. *Journal of Food Biochemistry, 37*(1), 36–44. https://doi.org/10.1111/j.1745-4514.2011.00604.x

Öztürk, C., & Küfrevioğlu, Ö.İ. (2024). Affinity gel synthesis from the p-aminobenzoic acid derivative 4-amino-2-methylbenzoic acid and purification of polyphenol oxidase from various plant sources. *Protein Expression and Purification, 219*, Article 106474. https://doi.org/10.1016/j.pep.2024.106474

Peng, W., Yao, F., Hu, J., Liu, Y., Lu, Z., Liu, Y., et al. (2018). Renewable protein-based monomer for thermosets: A case study on phthalonitrile resin. *Green Chemistry, 20*, 5158. https://doi.org/10.1039/C8GC01824C

Ren, Q.-Q., Yang, F., Ren, W., Wang, C., Jiang, W.-S., Zhao, Z.-Y., Chen, J., Lu, X.-Y., & Yu, Y. (2020). Amperometric biosensor based on Coimmobilization of multiwalled carbon nanotubes and horseradish peroxidase-gold nanocluster bioconjugates for detecting H2O2. *Journal of Nanomaterials, 2020*(1), Article 9627697. https://doi.org/10.1155/2020/9627697

Rezazade, M., Ketabi, S., & Qomi, M. (2024). Effect of functionalization on the adsorption performance of carbon nanotube as a drug delivery system for imatinib: Molecular simulation study. *BMC Chemistry, 18*, 85. https://doi.org/10.1186/s13065-024-01197-0

Şakiroğlu, H. (1994). *Kuşburnu meyvasından izole edilen polifenoloksidaz enziminin kinetik ve elektroforetik özelliklerinin incelenmesi (Ph.D. thesis, National Thesis Center of the Council of Higher Education, Türkiye)*. Thesis No: 35145.

Sarsenova, A., Demir, D., Çağlayan, K., Abiyev, S., Darbayeva, T., & Eken, C. (2023). Purification and properties of polyphenol oxidase of dried *Volvariella bombycina*. *Biology, 12*(1), 53. https://doi.org/10.3390/biology12010053

Sharif, N. (2024). Effects of pH on enzyme activity in Pakistan. *Journal of Chemistry, 3*(3), 49–59. https://doi.org/10.47672/jchem.2512

Siddiq, M., & Dolan, K. D. (2017). Characterization of polyphenol oxidase from blueberry (*Vaccinium corymbosum* L.). *Food Chemistry, 218*, 216–220. https://doi.org/10.1016/j.foodchem.2016.09.061

Thommes, M., Kaneko, K., Neimark, A. V., Olivier, J. P., Rodriguez-Reinoso, F., Rouquerol, J., & Sing, K. S. W. (2015). Physisorption of gases, with special reference to the evaluation of surface area and pore size distribution (IUPAC technical report). *Pure and Applied Chemistry, 87*(9–10), 1051–1069. https://doi.org/10.1515/pac-2014-1117

Tiwari, A., & Singh, V. (2007). Synthesis and characterization of electrical conducting chitosan-graft-polyaniline. *Express Polymer Letters, 5*, 308–317. https://doi.org/10.3144/expresspolymlett.2007.44

Ünal, M.Ü., Yabacı, S. N., & Şener, A. (2011). Extraction, partial purification and characterization of polyphenol oxidase from tea leaf (*Camellia sinensis*). *GIDA, 36*(3), 137–144.

Vesali Naseh, M., Khodadadi, A. A., Mortazavi, Y., Alizadeh Sahraei, O., Pourfayaz, F., & Mosadegh Sedghi, S. (2009). Functionalization of carbon nanotubes using nitric acid oxidation and DBD plasma. *International Journal of Chemical and Biological Engineering, 2*(2), 66–68.

Wang, Z., Yuan, J., Yang, J., Dong, Z., Yan, X., Yuan, C., et al. (2021). Effects of guankou grape polyphenol oxidase on enzymatic browning. *Journal of Food Processing and Preservation, 46*(1), Article e15471. https://doi.org/10.1111/jfpp.15471

Wee, Y., Park, S., Kwon, Y. H., Ju, Y., Yeon, K.-M., & Kim, J. (2019). Tyrosinase-immobilized CNT-based biosensor for highly sensitive detection of phenolic compounds. *Biosensors and Bioelectronics, 132*, 279–285. https://doi.org/10.1016/j.bios.2019.03.008

Whitney, P. L. (1974). Affinity chromatography of carbonic anhydrase. *Analytical Biochemistry, 57*(2), 467–476. https://doi.org/10.1016/0003-2697(74)90102-X

Yalçınkaya, F., Doğan, M., Bicil, Z., & Koçer Kızılduman, B. (2024). Effect of functionalization and Li-doping methods to hydrogen storage capacities of MWCNTs. *Fuel, 372*, Article 132274. https://doi.org/10.1016/j.fuel.2024.132274

Yanmaz, E., Doğan, M., & Turhan, Y. (2021). Effect of sodium dodecyl sulfate on thermal properties of polyvinyl alcohol (PVA)/modified single-walled carbon nanotube (SWCNT) nanocomposites. *Diamond and Related Materials, 115*, Article 108359. https://doi.org/10.1016/j.diamond.2021.108359Get

Yıldız, S., Bilen, Ç., & Karakuş, E. (2022). Purification of damson plum polyphenol oxidase by affinity chromatography and investigation of metal effects on enzyme activity. *Preparative Biochemistry & Biotechnology, 52*(9), 1019–1034. https://doi.org/10.1080/10826068.2021.2023825

Yu, K., He, W., Ma, X., Zhang, Q., Chen, C., Li, P., & Wu, D. (2024). Purification and biochemical characterization of polyphenol oxidase extracted from wheat bran (Wangrano). *Molecules, 29*, Article 1334. https://doi.org/10.3390/molecules29061334

Zaini, N. A. M., Osman, A., Hamid, A. A., Ebrahimpour, A., & Saari, N. (2013). Purification and characterization of membrane-bound polyphenoloxidase (mPPO) from snake fruit [*Salacca zalacca* (Gaertn.) Voss]. *Food Chemistry, 136*(2), 407–414. https://doi.org/10.1016/j.foodchem.2012.08.034

Zhang, T., Tang, M., Yao, Y., Ma, Y., & Pu, Y. (2019). MWCNT interactions with protein: Surface-induced changes in protein adsorption and the impact of protein corona on cellular uptake and cytotoxicity. *International Journal of Nanomedicine, 14*, 993–1009. https://doi.org/10.2147/IJN.S191689

Zou, C., Zhang, X., Xu, Y., & Yin, J. (2024). Recent advances regarding polyphenol oxidase in *Camellia sinensis*: Extraction, purification, characterization, and application. *Foods, 13*, 545. https://doi.org/10.3390/foods13040545